Inorganic Chemistry

pubs.acs.org/IC

Article

Magnetostructural and EPR Studies of Anisotropic Vanadium *trans*-Dicyanide Molecules

Mohamed R. Saber, Komalavalli Thirunavukkuarasu,* Samuel M. Greer, Stephen Hill,* and Kim R. Dunbar*

Cite This: *Inorg. Chem.* 2020, 59, 13262−13269

Read Online

ACCESS | Metrics & More | Article Recommendations | Supporting Information

ABSTRACT: A series of *trans*-dicyanide vanadium(III) compounds based on acetylacetonate, (PPN)[V^{III}(acac)$_2$(CN)$_2$]·(PPN)Cl·2MeCN (**1**), and salen ligands, (Et_4N)[V^{III}(salen)-(CN)$_2$] (**2a**), (PPN)[V^{III}(MeOsalen)(CN)$_2$]·DMF·2MeCN (**3**), and (PPN)[V^{III}(salphen)(CN)$_2$]·DMF (**4**) [salen = *N*,*N*′-ethylenebis(salicyl-imine), MeOsalen = *N*,*N*′-ethylenebis-(methoxysalicylimine), salphen = *N*,*N*′-phenylenebis(salicyl-imine), and PPN = bis(triphenylphosphine)iminium], were prepared and structurally characterized. High-field EPR studies reveal that the complexes exhibit moderate magnetic anisotropy with positive *D* values of +5.70, +3.80, +4.05, and +3.99 cm^{-1} for **1**−**4**, respectively.

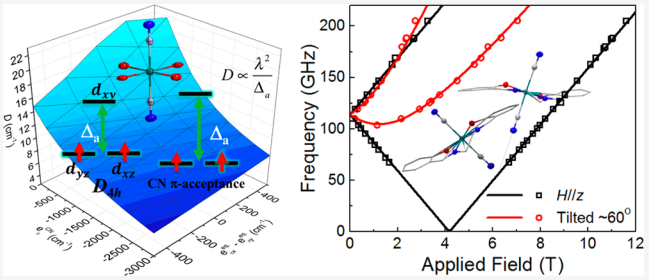

INTRODUCTION

The early 3d transition metals of groups 4−6 in cyanide environments are excellent candidates for developing molecules that exhibit strong exchange interactions, as shown in a theoretical paper by Ruiz and co-workers.[1] In particular, a cyanide environment is expected to promote strong exchange interactions due to increased π-back bonding into the cyanide π^* orbitals.[1−3] In support of this hypothesis is the fact that the combination of V^{II} (t_{2g}^3) and Cr^{III} (t_{2g}^3) spin centers in Prussian blue (PB) analogues has been found to lead to bulk magnetic ordering well above room temperature.[4−6]

Of specific interest to the current study is the fact that the vanadium(III) ion is known to participate in strong ferromagnetic superexchange interactions in dinuclear species[7,8] and often exhibits sizable magnetic anisotropy, with negative axial zero-field splitting (ZFS) parameters, |*D*|, of up to 20 cm^{-1}.[8−10] These attributes poise V^{III} building blocks to be excellent prospects for bistable systems such as single-molecule magnets (SMMs) and single-chain magnets (SCMs), and for molecular magnets in general.[11] Indeed, Sessoli and co-workers were able to achieve an increase of the spin state and a significant enhancement of SMM properties by replacing the central iron(III) ion with vanadium(III) in a tetrairon(III) cluster.[11]

Despite the advantages that one could obtain by incorporating V^{III} ions into molecular magnets containing cyanide, there are only a few well-known vanadium cyanide building blocks,[12−17] specifically $K_4[V(CN)_6]$,[12] $K_3[VO(CN)_5]$,[13] $K_4[V(CN)_7]\cdot 2H_2O$,[16] and $(Et_4N)_3[V(CN)_6]$,[17] most likely due to the tendency for low valent vanadium complexes to decompose in the presence of oxygen and water.[18−25] Indeed, the incorporation of the hexacyanovanadate(III) anion $[V^{III}(CN)_6]^{3-}$ into PB-type materials has proven to be difficult because of the ease of oxidation of V^{III} to V^{IV},[26] but the room temperature cyanide-based magnet, $V^{II}_{0.42}V^{III}_{0.58}[Cr^{III}(CN)_6]_{0.86}\cdot 2.8H_2O$ (T_C = 315 K), reported by Verdaguer's group is a notable example of a vanadium containing molecule-based extended magnet.[6] It is also important to point out that the first room temperature molecule-based magnet, $V(TCNE)_2$ (T_C = 350 K), reported by Miller et al. is also based on vanadium, albeit V^{II} and not V^{III}.[27]

Molecules that contain cyanovanadate building blocks are quite rare.[24,25] The only example of a discrete cyanide-bridged molecule containing V^{III} is the one reported by Long and co-workers who demonstrated that the reaction of [(cyclen)V-$(CF_3SO_3)_2$](CF_3SO_3) with (Et_4N)CN in DMF produces the tetrahedral cage complex, $[(cyclen)_4V_4(CN)_6]^{6+}$, which exhibits relatively strong antiferromagnetic coupling, resulting in a ground state spin of S = 0.[24]

We have a longstanding interest in the incorporation of anisotropic early transition-metal centers into discrete cyanide-based molecules,[28,29] an example of which is the synthesis and magnetic studies of a new early transition-metal cyanide building block based on Ti^{III}.[30] As part of our pursuit of new V^{III} dicyanide building blocks, we elected to use salen type

Received: June 2, 2020
Published: September 1, 2020

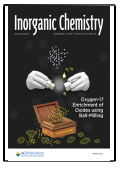

https://dx.doi.org/10.1021/acs.inorgchem.0c01595
Inorg. Chem. 2020, 59, 13262−13269

[(salen = *N*,*N*′-ethylenebis(salicylimine), MeOsalen = *N*,*N*′-ethylenebis(methoxysalicylimine), salphen = *N*,*N*′-phenylenebis(salicyl-imine)], and acac (acac = acetylacetonate) ligands. Salen-type cyanide building blocks are known for a number of metals,[31−37] including the $[Ru^{III}salen(CN)_2]^-$ molecule which has been incorporated into several interesting heterometallic cyanide clusters.[38,39] The diketonate family has also been used as capping ligands for cyanide compounds with Ru^{III} and Co^{III}.[38−44]

Herein, we report the syntheses, structural characterization, spectroscopic studies, as well as magnetic and EPR measurements of new anisotropic vanadium dicyanide building blocks with acac- and salen-based ligands with axial coordination geometries.

RESULTS AND DISCUSSION

Syntheses and Characterization. V^{III} precursors of general formulas $[V^{III}(L)Cl(THF)]$ (L = salen ligand), $[V^{III}(acac)Cl_2(THF)_2]$, and $[V^{III}(acac)_2Cl(THF)]$ are used to prepare cyanide derivatives.[45−48] The reaction of $[V^{III}(acac)_2Cl(THF)]$ with two equivalents of (PPN)CN in acetonitrile afforded yellow crystals of $(PPN)[V^{III}(acac)_2(CN)_2]\cdot(PPN)Cl\cdot 2MeCN$ (**1**) (Figures 1 and S1), which involves cocrystallization with an equivalent of (PPN)Cl (PPN = bis(triphenylphosphine)iminium). Attempts to prepare the $(Et_4N)[V^{III}(acac)_2(CN)_2]$ compound by reacting $[V^{III}(acac)_2Cl(THF)]$ with two equivalents of $(Et_4N)CN$ in acetonitrile resulted in yellow crystals of $(Et_4N)_2[V^{III}(acac)(CN)_4]$ as determined by X-ray measurements. These results indicate a tendency for the acac ligands to be labilized. In an analogous fashion, the salen precursors were reacted with two equivalents of (PPN)CN or $(Et_4N)CN$ in DMF/MeCN to prepare the corresponding dicyanide complexes, $(Et_4N)[V^{III}(salen)(CN)_2]$ (**2a**), $(PPN)[V^{III}(salen)(CN)_2]$ (**2b**), $(PPN)[V^{III}(MeOsalen)(CN)_2]\cdot DMF\cdot 2MeCN$ (**3**), and $(PPN)[V^{III}(salphen)(CN)_2]\cdot DMF$ (**4**).

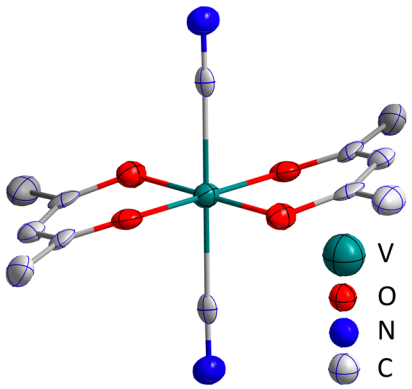

Figure 1. Molecular structure of the $[V^{III}(acac)_2(CN)_2]^-$ anion in **1**. Thermal ellipsoids are drawn at the 50% probability level. Hydrogen atoms have been omitted for the sake of clarity.

Compound **1** crystallizes in the triclinic $P\bar{1}$ space group (Table S1) with the anion consisting of a vanadium center with four equatorial O atoms from two acac ligands and two carbon atoms from axial cyanide ligands (Figure 1). The charge on the anion is balanced by one PPN^+ cation, but there are also additional equivalents of (PPN)Cl and two acetonitrile solvent molecules in the structure. Selected bond distances and angles are listed in Table S2. The V(1)−O bond distances of 1.966(2) Å and 1.978(2) Å are in the usual range of reported V^{III} diketonate complexes.[49] The V(1)—C≡N distance of 2.168(2) Å is slightly longer than the corresponding distances reported for $(Et_4N)_3[V(CN)_6]$[17] [2.127(3) Å], $K_4[V(CN)_7]\cdot 2H_2O$[16] [2.147(7) Å], $(Et_4N)[Tp^*V(CN)_3]$[25] [2.085(7) Å], and $[(cyclen)V(CN)_3]$[24] [2.160(6) Å]. The cyanide ligands are nearly linear with a V—C≡N angle of 179.6(2)°; the C≡N bond distance of 1.150(3) Å is typical for vanadium cyanide complexes.[12−16,24,25] The chelate ring of the acetylacetonate ligand is twisted out of the coordination plane with a dihedral angle of ∼19.2°.

Similarly, the salen-containing compounds exhibit a pseudo-octahedral environment around the central vanadium in the anion, with the N_2O_2 donor atoms of the salen ligand occupying the equatorial coordination sites, while the axial sites are occupied by carbon donors of axial cyanide ligands (Figures 2a, S2, and S3). The charge on the anion is balanced by $(Et_4N)^+$ in **2a** and $(PPN)^+$ in **2b**. Selected bond distances and angles are compiled in Table S2. Compound **2a** crystallizes in the orthorhombic space group *Fdd*2 (Table S1). It exhibits a V(1)−O(1) bond distance of 1.921(2) Å and a V(1)−N(2) bond distance of 2.094(2) Å. These values are comparable to those observed for previously reported vanadium salen complexes.[50] The metal cyanide distance, V(1)—C≡N = 2.178(3) Å, is slightly longer than that found in **1**, and the average C≡N bond distance is 1.159(3) Å. The cyanide ligands are slightly bent at an average V—C≡N angle of 175.9(2)°. Compound **2b** (Figure S3) crystallizes in the orthorhombic space group *Pcca* (Table S1). The $[V^{III}salen(CN)_2]^-$ anion exhibits very similar bond distances and

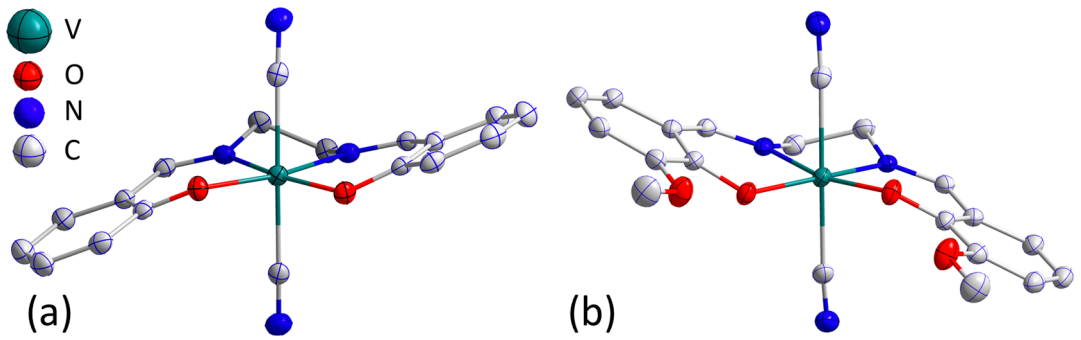

Figure 2. Molecular structure of (a) the $[V^{III}(salen)(CN)_2]^-$ anion in **2** and (b) the $[V^{III}(MeOsalen)(CN)_2]^-$ anion in **3**. Thermal ellipsoids are drawn at the 50% probability level. Hydrogen atoms have been omitted for the sake of clarity.

https://dx.doi.org/10.1021/acs.inorgchem.0c01595
Inorg. Chem. 2020, 59, 13262−13269

angles to **2a** [V(1)—O(1) = 1.9133(10) Å, V(1)—N(2) = 2.0990(12) Å, V(1)—C≡N = 2.1898(15) Å, and V—C≡N = 173.32(13)° (Table S2)]. The N,O chelate ring of the salen ligand exhibits a dihedral angle with the metal coordination plane of 19.848(6)° in **2a** and 22.01(1)° in **2b**.

Compound **3** crystallizes in the monoclinic space group $P2_1/c$ (Table S1) with a similar pseudo-octahedral coordination environment for the complex anion, with the N_2O_2 donor atoms of the MeOsalen ligand in the equatorial coordination sites and carbon donors of the cyanide ligands in the axial positions (Figures 2b and S4). The bond distances [V(1)—O(1) = 1.909(2) Å and V(1)—N(2) = 2.082(2) Å] are very similar to those of **2a**, whereas the metal cyanide distance [V(1)—C≡N = 2.178(3) Å] and the C≡N bond lengths [1.145(4) Å] are slightly shorter. The V—C≡N angle of 172.0(3)° is also slightly more bent than in the case of **2a**, while the N,O chelate ring of the MeOsalen ligand forms a similar dihedral angle with the coordination plane of 23.633(6)° (Table S2), similar to related octahedral V^{III} salen moeties.[50,51] The crystal contains two partially occupied disordered acetonitrile molecules and a DMF molecule of crystallization.

Compound **4** crystallizes in the monoclinic space group $P2_1/c$ (Table S1) with a pseudo-octahedral environment for the complex anion (Figures 3 and S5). The bond distances

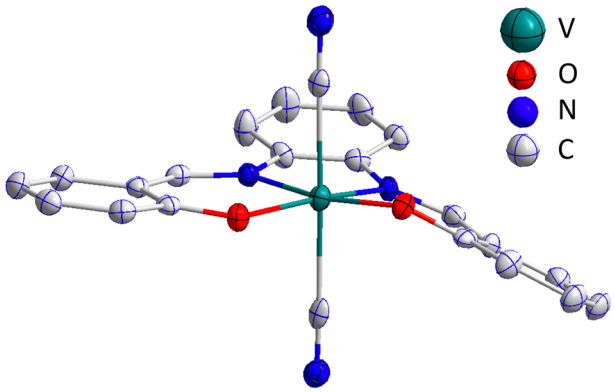

Figure 3. Molecular structure of the $[V^{III}(salphen)(CN)_2]^-$ anion in **4**. Thermal ellipsoids are drawn at the 50% probability level. Hydrogen atoms have been omitted for the sake of clarity.

[V(1)–O(1) = 1.9034(16) Å, V(1)–O(2) = 1.8997(16) Å, V(1)–N(3) = 2.082(2) Å, V(1)–N(4) = 2.1114(19) Å] and average metal cyanide distance V(1)—C≡N = 2.172(2) Å are very close to those in **2a**, while the average C≡N bond distance is 1.152(3) Å. The cyanide ligands are slightly bent with a V—C≡N angle of 176.7(2)°, whereas the N,O chelate ring of the salphen ligand forms a dihedral angle of 25.780(6)° with the coordination plane. The crystal contains a disordered DMF molecule of crystallization.

The IR spectra of the compounds (Table S3) are consistent with the presence of terminal cyanides as indicated by the ν(C≡N) stretching frequencies at 2045 cm^{-1} in **1** and in the 2100–2104 cm^{-1} range in **2**–**4**. Surprisingly, the ν(C≡N) stretching mode for **1** is shifted to a lower frequency compared to the corresponding modes observed for simple cyanide salts, whereas for **2**–**4**, the vibration shifts to higher frequencies and lies within the range of other reported vanadium cyanide precursors.[12–16,25] The presence of the coordinated Schiff base ligands in **2**–**4** is indicated by the ν(C═N) stretching frequencies of the imine group at 1618–1666 cm^{-1}.

Magnetic Studies. Magnetic measurements were performed on crushed crystals at an applied magnetic field, H = 1000 Oe, over a temperature range, T = 1.8 to 300 K. The χT versus T plot for **1** (Figure 4) reveals a room temperature value

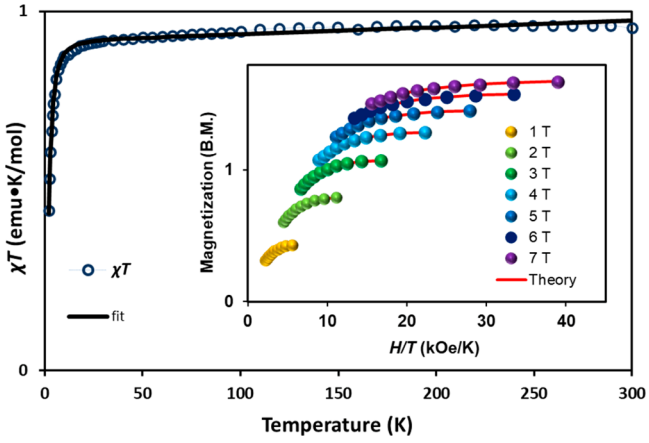

Figure 4. Temperature dependence of the χT product (δ) for **1**. The solid line corresponds to the best fit using PHI (see main text). Inset: Reduced magnetization of **1**. Solid lines correspond to the best-fit using ANISOFIT2.0.

of 0.96 emu·K·mol^{-1}, corresponding to an isolated V^{III} ion with S = 1, a Landé factor g = 1.94, and a temperature-independent paramagnetism (TIP) contribution of 1.0 × 10^{-4} emu·mol^{-1}. Upon lowering the temperature, χT gradually decreases until ~15 K is reached, after which it sharply drops to 0.43 emu·K·mol^{-1} at 2 K, indicating ZFS effects. The temperature dependence of the χT product over the 2–300 K range was fit using the program PHI[52] to the following spin Hamiltonian:

$$\hat{H} = D(\hat{S}_z^2 - S(S+1)/3) + E(\hat{S}_x^2 - \hat{S}_y^2) + g\mu_B\mu_0\vec{H}\cdot\hat{S} \quad (1)$$

where $\hat{S}$ is the spin operator with components $\hat{S}_i$ (i = x, y, z), μ_0 is the vacuum permeability, and μ_B is the Bohr magneton, yielding axial and rhombic ZFS parameters, D = +5.72 cm^{-1} and E = +0.41 cm^{-1} (E/D = 0.072), respectively, and isotropic g = 1.92. Field-dependent reduced magnetization data at temperatures between 1.8 and 4.5 K reveal nonsuperimposable iso-field lines when plotted versus H/T due to the presence of ZFS interactions (Figure 4, inset). Fits using ANISOFIT2.0[53] led to estimates of the ZFS parameters for **1** of D = +5.6 cm^{-1} and E = 0.14 cm^{-1} (E/D = 0.025), with g = 1.96, which are quite similar to the PHI results. The lack of saturation of the magnetization, even at 7 T, is not unexpected due to the anisotropic nature of the V^{III} center, but approaches the expected value of ~2μ_B. A similar behavior, consistent with isolated anisotropic V^{III} centers, was observed for **2a**, **2b**, **3**, and **4** (Figures S6–S9). Fits of χT and reduced magnetization data led to ZFS parameters, D = +5.3, +3.97, +4.2, and +4.3 cm^{-1} for **2a,b**–**4**, respectively, with E ~ 0 in each case, to within the uncertainty of the fits. The fit for **2a** indicates the presence of intermolecular antiferromagnetic interactions (zJ = −0.33 cm^{-1}), presumably due to the smaller size of the Et_4N^+ cations [V···V separation of 7.734(1) Å] as compared to the significantly larger PPN^+ cations in the other samples [V···V = 10.496(1) Å in **2b**].

https://dx.doi.org/10.1021/acs.inorgchem.0c01595
Inorg. Chem. 2020, 59, 13262–13269

EPR Studies. While magnetic measurements can, in theory, provide estimates of ZFS parameters, inaccuracies often arise due to insufficient constraints provided by bulk thermodynamic data.[54] It is better to use a spectroscopic technique such as EPR (in this case, high-field EPR due to the sizable ZFS energies involved),[55,56] which directly measures energy splittings that can be related to ZFS parameters in a straightforward manner.

Multifrequency high-field EPR measurements in magnetic fields up to 14.5 T were performed on powder samples[57] of all compounds, except for **2**, where **2a** was measured as a single-crystal.[58] Representative spectra for **2a** are shown for several different frequencies in Figure 5a. An angle-dependent study

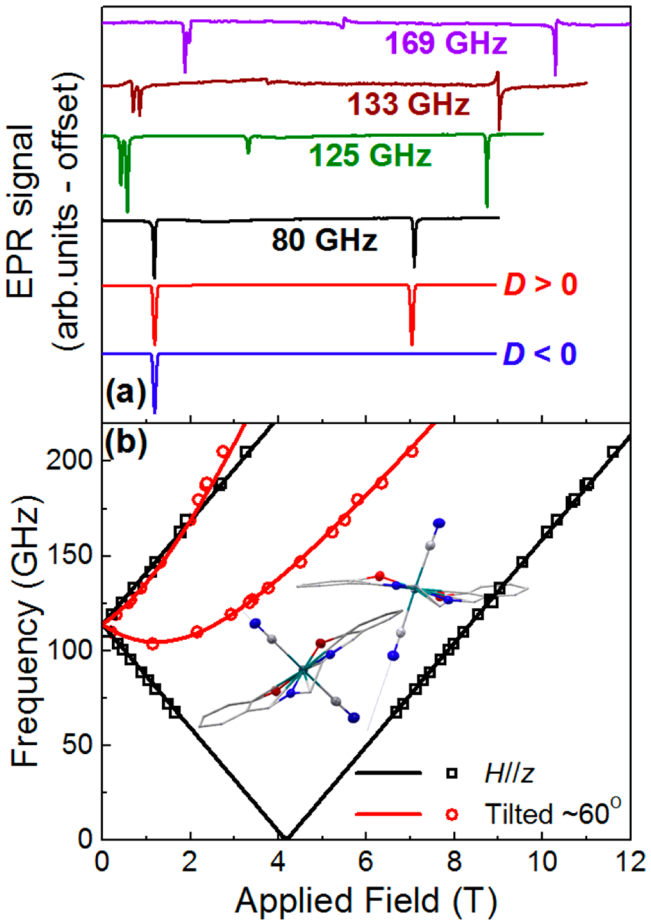

Figure 5. (a) Oriented single-crystal high-field EPR spectra recorded for **2a** at multiple high-frequencies at a temperature of 1.5 K. (b) 2D plot of frequency versus resonance position. The red lines in (b) correspond to a second vanadium center tilted by ~60°; the inset depicts two V^{III} centers in the crystal structure with an angle of ~65° between their respective C−V−C axes. The lower two traces in (a) are simulations of the 80 GHz, 1.5 K spectrum for both signs of *D*, confirming its positive sign.

was first performed (Figures S10 and S11) in order to orient the crystal such that the applied magnetic field was aligned as close as possible to the local *z*- (or hard-, *vide infra*) axis associated with one of the two distinct molecular orientations within the unit cell.[59] To extract the spin Hamiltonian parameters, the peak positions observed for each frequency were gathered in a 2D plot of frequency versus resonant magnetic field (Figure 5b) and fit to eq 1.

The first thing to note from Figure 5 is the high-quality of the crystal, which gives extremely sharp resonances for a transition-metal complex with such a large magnetoanisotropy. This enables clear resolution of two sets of resonances corresponding to the two distinct molecular orientations. As seen in Figure 5b, the open squares (□) exhibit a purely linear field dependence indicative of a diagonal Hamiltonian, confirming that the applied field is parallel to the *z*-axis of the ZFS tensor. Also notable is the absence of any breaking of the degeneracy of the two branches that intercept the zero-field axis at 114 GHz. This observation confirms that the rhombic ZFS parameter $E = 0$ for **2a** (see also Figure S12), to within the resolution of the measurement (<0.03 cm^{-1}). Therefore, the zero-field intercept exactly gives the *D* parameter (= 3.80 cm^{-1}) for **2a**. Meanwhile, 80 GHz simulations displayed in the lower portion of Figure 5a for both signs of *D* confirm that the anisotropy is of the easy-plane type ($D > 0$). Finally, the open circles (○) in Figure 5b, corresponding to the other molecular orientation, give the best simulation with a tilt angle of ~60° with respect to the aligned molecules (see also Figure S11), information that is only accessible via single-crystal measurements. This is supported by examination of the unit cell which indeed shows two molecules with ~65° separating their C−V−C axes (Figure 5b inset). This observation suggests that the *z*-axis of the ZFS tensor is nearly aligned with the C−V−C axes.

Analyses of multifrequency EPR spectra obtained for powders of compounds **1**, **3**, and **4** proceeded similarly, but they considered all of the canonical turning points in the powder average. The spectra, along with 2D frequency versus resonant field plots ("Florida maps"), are reported in the Supporting Information (Figures S13−S16). The ZFS parameters obtained from the EPR fits are listed in Table 1.

Table 1. EPR Spin Hamiltonian Parameters for Compounds 1−4

compound	*g*(*x*,*y*,*z*)	*D* (cm^{-1})	*E* (cm^{-1})
1	1.93, 1.96, 1.98	+5.70	0.73
2a[a]	1.93, 1.93, 1.95	+3.80	0
3	1.95, 1.95, 1.99	+4.05	0
4	1.95, 1.95, 1.98	+3.99	0

[a]The *g* values are calculated based on the relative crystal alignment assuming a tilt angle of 60°.

The axial ZFS parameter, *D*, was found to be positive in all cases, lying in the +3.8 to +5.7 cm^{-1} range. The rhombic term, *E*, is absent in all compounds except for **1**, where it is substantial (~0.73 cm^{-1} or $E/D = 0.13$). For this reason, we constrained $g_x = g_y$ for all compounds except **1**. The obtained parameters are comparable to those for previously reported V^{III} complexes with positive axial anisotropy (~5 $cm^{-1} \leq D \leq 7$ cm^{-1}), e.g., $K_3V^{III}(ox)_3 \cdot 3H_2O$ (D = +5.3 cm^{-1}),[60] $V^{III}(acac)_3$ (D = +6.9 cm^{-1}),[61] $[V^{III}(urea)_6](ClO_4)_3$ (D = +6.0 cm^{-1}),[62] and $Cs[Ga:V](SO_4)_2 \cdot 12H_2O$ (D = +4.77 cm^{-1}).[63]

THEORY AND DISCUSSION

To relate the experimentally determined ZFS parameters to the physical structure of the compounds, we developed a model based on ligand field (LF) theory. The π-accepting nature of the CN^- ligands results in the stabilization of the *xz*/*yz* orbital pair and, thus, a ground state configuration of $|(xz)^1(yz)^1|$ (Figure 6). In this scenario the largest contribution to the ZFS is positive and originates from the spin−orbit

https://dx.doi.org/10.1021/acs.inorgchem.0c01595
Inorg. Chem. 2020, 59, 13262−13269

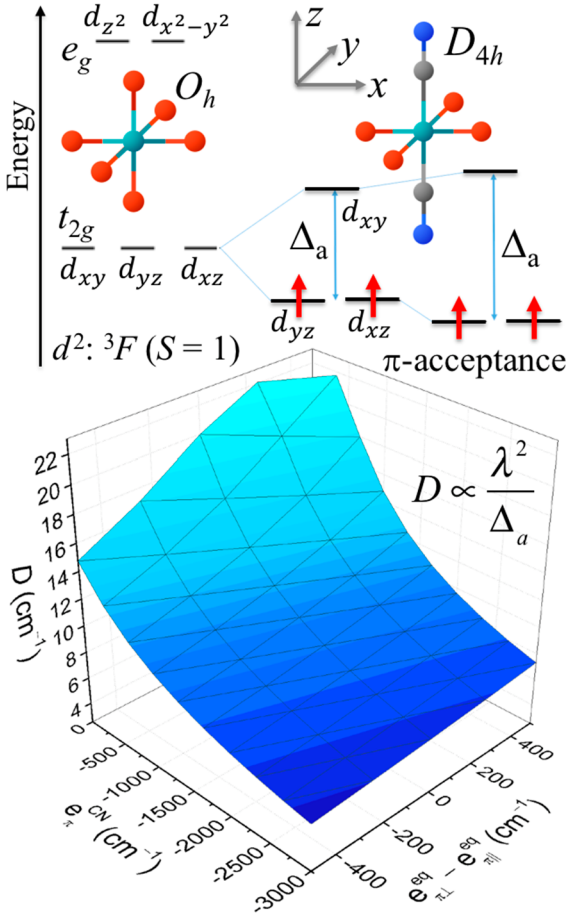

Figure 6. Top-left diagram shows the relative *d*-orbital splitting due to an octahedral (O_h) LF. The effect of a tetragonal distortion (magnitude Δ_a) on the three lowest-lying t_{2g} orbitals is shown to the right, followed by the effect of the π-accepting nature of the ligands. This model relies on multiple coordinate frames (see Figure S17). Within the molecular frame, the *z*-axis coincides with the vector formed by the V−CN bonds, while the *x*- and *y*-axes coincide with the coordinating atoms in the equatorial plane. This qualitative model assumes local D_{4h} symmetry, i.e., the equatorial atoms are equivalent. The π-bonding interaction involving the CN^- ligands (e^{π}_{CN}) is isotropic with respect to *x* and *y*. Likewise, the D_{4h} symmetry ensures that this is also the case for the equatorial ligands. However, we allow the equatorial π-bonding interaction to be anisotropic with respect to the in-plane (*xy* or ||) and out-of-plane (*z* or ⊥) directions, i.e., $e^{\pi\parallel}_{eq} \neq e^{\pi\perp}_{eq}$. The 3D surface plot (lower figure) shows the variation of the *D* parameter as a function of both the π-accepting strength of the apical CN^- ligands (e^{π}_{CN}) and the anisotropic interaction of the equatorial ligands ($e^{\pi\perp}_{eq} \neq e^{\pi\parallel}_{eq}$).

interaction of the ground state with the doubly degenerate first excited state ($|(xz)^1(xy)^1|$, $|(yz)^1(xy)^1|$). The magnitude of this contribution to *D* is proportional to λ^2/Δ_a, where λ is the many electron spin−orbit coupling constant and Δ_a is approximately equal to the energy difference between the *xz*/*yz* and *xy* orbitals. The π-interactions with the equatorial ligands also affect the value of Δ_a. The salen and acac ligands will behave as anisotropic π donors, meaning that the strength of the π interaction in the plane of the ligand ($\pi_\parallel$) will be different from the one out of the plane ($\pi_\perp$). These two interactions will have competing effects on the magnitude of Δ_a and, in turn, the anisotropy of the system. The $\pi_\perp$ interaction destabilizes the *xz*/*yz* orbital pair, bringing them closer to the *xy* orbital, resulting in a larger *D*. If this interaction becomes strong compared to the CN^- back-bonding interaction, then the orbital ordering could become reversed making the *xy* orbital lowest in energy. Conversely, the $\pi_\parallel$ component will destabilize the *xy* orbital, thus increasing Δ_a and lowering *D*. To illustrate these effects, we performed a series of LF theory calculations based on the angular overlap model (AOM).[64,65] It should be noted that the obtained results, which are shown in Figure 6, are approximate in that they consider only the ^3F state and assume rigorous D_{4h} symmetry. A comparison with the experimentally determined *D* values, and assuming a constant ratio of the $\pi_\perp/\pi_\parallel$-interaction strength, is in accord with the expectation that salen-based ligands are weaker π-donors than the acac ligand. The observed ZFS parameters also underscore the importance of ligand rigidity in the salen complexes to suppress the rhombic distortion resulting in an $E \approx 0$, as compared to the less rigid acac ligand with a nonzero rhombic term.

CONCLUSIONS

A family of new anisotropic vanadium cyanide building blocks based on acetylacetonate, salen [*N*,*N*′-ethylenebis (salicylimine)], 2-methoxysalen [*N*,*N*′-ethylenebis(2-methoxysalicylimine)], and salphen [*N*,*N*′-phenylenebis (salicylimine)], were prepared. Magnetic and high-field EPR studies revealed moderate positive ZFS parameters, e.g., D = +5.70, +3.80, +4.05, and +3.99 cm^{-1} for **1**−**4**, respectively, which approximately follow the variation in the LF strength of the capping ligands. The results highlight the importance of ligand rigidity for suppressing rhombic distortions. Attempts to incorporate these building blocks into cyanide bridged chains are in progress.

ASSOCIATED CONTENT

Supporting Information

The Supporting Information is available free of charge at https://pubs.acs.org/doi/10.1021/acs.inorgchem.0c01595.

Additional crystallographic, spectroscopic, magnetic and EPR data, as well as details of the theoretical model employed (PDF)

Accession Codes

CCDC 2004189−2004193 contain the supplementary crystallographic data for this paper. These data can be obtained free of charge via www.ccdc.cam.ac.uk/data_request/cif, or by emailing data_request@ccdc.cam.ac.uk, or by contacting The Cambridge Crystallographic Data Centre, 12 Union Road, Cambridge CB2 1EZ, UK; fax: +44 1223 336033.

AUTHOR INFORMATION

Corresponding Authors

Komalavalli Thirunavukkuarasu − *Department of Physics, Florida A&M University, Tallahassee, Florida 32307, United States; National High Magnetic Field Laboratory, Florida State University, Tallahassee, Florida 32310, United States;* orcid.org/0000-0001-6148-2670; Email: komalavalli.thirunav@famu.edu

Stephen Hill − *National High Magnetic Field Laboratory and Department of Physics, Florida State University, Tallahassee, Florida 32310, United States;* orcid.org/0000-0001-6742-3620; Email: shill@magnet.fsu.edu

Kim R. Dunbar − *Department of Chemistry, Texas A&M University, College Station, Texas 77842-3012, United States;*

https://dx.doi.org/10.1021/acs.inorgchem.0c01595
Inorg. Chem. 2020, 59, 13262−13269

orcid.org/0000-0001-5728-7805; Email: dunbar@mail.chem.tamu.edu

Authors

Mohamed R. Saber − *Department of Chemistry, Texas A&M University, College Station, Texas 77842-3012, United States; Chemistry Department, Faculty of Science, Fayoum University, Fayoum 63514, Egypt;* orcid.org/0000-0002-4707-1362

Samuel M. Greer − *National High Magnetic Field Laboratory and Department of Chemistry & Biochemistry, Florida State University, Tallahassee, Florida 32310, United States;* orcid.org/0000-0001-8225-3252

Complete contact information is available at: https://pubs.acs.org/10.1021/acs.inorgchem.0c01595

Notes

The authors declare no competing financial interest.

■ ACKNOWLEDGMENTS

K.R.D. thanks the National Science Foundation (NSF CHE-1808779) and the Welch Foundation (A-1449) for financial support. S.M.G. acknowledges support from the NSF Graduate Research Fellowship Program (DGE-1449440). K.T. acknowledges a Feodor−Lynen Fellowship from the Alexander von Humboldt Foundation. Work performed at the NHMFL was supported by the NSF (DMR-1157490, DMR-1610226, and DMR-1644779) and the State of Florida.

■ REFERENCES

(1) Ruiz, E.; Rodriguez-Fortea, A.; Alvarez, S.; Verdaguer, M. Is it Possible to Get High T_C Magnets With Prussian Blue Analogues? A Theoretical Prospect. *Chem. - Eur. J.* **2005**, *11*, 2135−2144.

(2) Entley, W. R.; Girolami, G. S. High-Temperature Molecular Magnets Based on Cyanovanadate Building-Blocks - Spontaneous Magnetization at 230 K. *Science* **1995**, *268*, 397−400.

(3) Weihe, H.; Gudel, H. U. Magnetic Exchange Across the Cyanide Bridge. *Comments Inorg. Chem.* **2000**, *22*, 75−103.

(4) Hatlevik, O.; Buschmann, W. E.; Zhang, J.; Manson, J. L.; Miller, J. S. Enhancement of the Magnetic Ordering Temperature and Air Stability of a Mixed Valent Vanadium Hexacyanochromate(III) Magnet to 99 °C (372 K). *Adv. Mater.* **1999**, *11*, 914−918.

(5) Holmes, S. M.; Girolami, G. S. Sol-Gel Synthesis of $KV^{II}[Cr^{III}(CN)_6].2H_2O$: A Crystalline Molecule-Based Magnet with a Magnetic Ordering Temperature Above 100 °C. *J. Am. Chem. Soc.* **1999**, *121*, 5593−5594.

(6) Ferlay, S.; Mallah, T.; Ouahes, R.; Veillet, P.; Verdaguer, M. A room-temperature organometallic magnet based on Prussian blue. *Nature* **1995**, *378*, 701−703.

(7) Shaw, R.; Tuna, F.; Wernsdorfer, W.; Barra, A. L.; Collison, D.; McInnes, E. J. L. Large spin, magnetically anisotropic, octametallic vanadium(III) clusters with strong ferromagnetic coupling. *Chem. Commun.* **2007**, 5161−5163.

(8) Knopp, P.; Wieghardt, K.; Nuber, B.; Weiss, J.; Sheldrick, W. S. Syntheses, electrochemistry, and spectroscopic and magnetic-properties of new mononuclear and binuclear complexes of vanadium(III), -(IV), and -(V) containing the tridentate macrocycle 1,4,7-trimethyl-1,4,7-triazacyclononane (L) - Crystal structures of $[L_2V_2(acac)_2((-O)]I_2.2H_2O$, $[L_2V_2O_4((-O)].14H_2O$, and $[L_2V_2O_2(OH)_2((-O)](ClO_4)_2$. *Inorg. Chem.* **1990**, *29*, 363−371.

(9) Tidmarsh, I. S.; Batchelor, L. J.; Scales, E.; Laye, R. H.; Sorace, L.; Caneschi, A.; Schnack, J.; McInnes, E. J. Tri-, tetra- and octametallic vanadium(III) clusters from new, simple starting materials: interplay of exchange and anisotropy effects. *Dalton Trans.* **2009**, 9402−9409.

(10) Krzystek, J.; Fiedler, A. T.; Sokol, J. J.; Ozarowski, A.; Zvyagin, S. A.; Brunold, T. C.; Long, J. R.; Brunel, L. C.; Telser, J. Pseudooctahedral Complexes of Vanadium(III): Electronic Structure Investigation by Magnetic and Electronic Spectroscopy. *Inorg. Chem.* **2004**, *43*, 5645−5658.

(11) Westrup, K. C.; Boulon, M. E.; Totaro, P.; Nunes, G. G.; Back, D. F.; Barison, A.; Jackson, M.; Paulsen, C.; Gatteschi, D.; Sorace, L.; Cornia, A.; Soares, J. F.; Sessoli, R. Adding Remnant Magnetization And Anisotropic Exchange to Propeller-like Single-Molecule Magnets through Chemical Design. *Chem. - Eur. J.* **2014**, *20*, 13681−13691.

(12) Jagner, S.; Németh, A.; Klewe, B.; Granberg, M.; Karlsson, F.; Edlund, K.; Eliasen, M.; Herskind, C.; Laursen, T.; Pedersen, P. M. Crystal-Structure of Potassium Hexacyanovanadate(II), $K_4[V(CN)_6]$. *Acta Chem. Scand.* **1975**, *29a*, 255−264.

(13) Jagner, S.; Vannerberg, N.-G.; Kenne, L.; Pilotti, A.; Svensson, S.; Swahn, C.-G. Crystal-Structure of Potassium Oxopentacyanovanadate(IV), $K_3[VO(CN)_5]$. *Acta Chem. Scand.* **1973**, *27*, 3482−3498.

(14) Nelson, K. J.; Miller, J. S. Incorporation of Substitutionally Labile $[V^{III}(CN)_6]^{3-}$ into Prussian Blue Type Magnetic Materials. *Inorg. Chem.* **2008**, *47*, 2526−2533.

(15) Schmid, V.; Linder, R.; Marian, C. M. The UV/Vis Spectrum of Potassium Heptacyanovanadate(III): A Theoretical Multi-Reference Configuration Interaction Study Combined with Low-Temperature Experiments. *Eur. J. Inorg. Chem.* **2006**, *2006*, 1588−1593.

(16) Towns, R. L. R.; Levenson, R. A. Structure of the seven-coordinate cyano complex of vanadium(III). *J. Am. Chem. Soc.* **1972**, *94*, 4345−4346.

(17) Nelson, K. J.; Giles, I. D.; Troff, S. A.; Arif, A. M.; Miller, J. S. Solvent-Enhanced Magnetic Ordering Temperature for Mixed-Valent Chromium Hexacyanovanadate(II), $Cr^{II}_{0.5}Cr^{III}[V^{II}(CN)_6]\cdot zMeCN$, Magnetic Materials. *Inorg. Chem.* **2006**, *45*, 8922−8929.

(18) Kumagai, H.; Kitagawa, S. Synthesis and Structure of Novel Vanadium(III) Compounds Having a Cyclic Core. *Chem. Lett.* **1996**, *25*, 471−472.

(19) Castro, S. L.; Sun, Z.; Grant, C. M.; Bollinger, J. C.; Hendrickson, D. N.; Christou, G. Single-Molecule Magnets: Tetranuclear Vanadium(III) Complexes with a Butterfly Structure and an S = 3 Ground State. *J. Am. Chem. Soc.* **1998**, *120*, 2365−2375.

(20) Papoutsakis, D.; Grohol, D.; Nocera, D. G. Magnetic Properties of a Homologous Series of Vanadium Jarosite Compounds. *J. Am. Chem. Soc.* **2002**, *124*, 2647−2656.

(21) Dujardin, E.; Ferlay, S.; Phan, X.; Desplanches, C.; Cartier dit Moulin, C.; Sainctavit, P.; Baudelet, F.; Dartyge, E.; Veillet, P.; Verdaguer, M. Synthesis and Magnetization of New Room-Temperature Molecule-Based Magnets: Effect of Stoichiometry on Local Magnetic Structure by X-ray Magnetic Circular Dichroism. *J. Am. Chem. Soc.* **1998**, *120*, 11347−11352.

(22) Zhou, P. H.; Xue, D. S.; Luo, H. Q.; Yao, J. L.; Shi, H. G. Preparation and characterization of highly ordered vanadium-iron cyanide molecular magnet nanowire arrays. *Nanotechnology* **2004**, *15*, 27−31.

(23) Verdaguer, M.; Bleuzen, A.; Train, C.; Garde, R.; Fabrizi de Biani, F.; Desplanches, C. Room-temperature molecule-based magnets. *Philos. Trans. R. Soc., A* **1999**, *357*, 2959−2976.

(24) Lee, I. S.; Long, J. R. Synthesis and magnetic behavior of the tetrahedral cage complex $[(cyclen)_4V_4(CN)_6]^{6+}$. *Dalton Trans.* **2004**, 3434−3436.

(25) Li, D. F.; Parkin, S.; Wang, G. B.; Yee, G. T.; Holmes, S. M. Early Metal Di- and Tricyanometalates: Useful Building Blocks for Constructing Magnetic Clusters. *Inorg. Chem.* **2006**, *45*, 2773−2775.

(26) Nelson, K. J.; Daniels, M. C.; Reiff, W. M.; Troff, S. A.; Miller, J. S. $[Cr_3(NCMe)_6]^{3+}$ - a Labile Cr^{III} Source Enabling Formation of $Cr[M(CN)_6]$ (M = V, Cr, Mn, Fe) Prussian Blue-Type Magnetic Materials. *Inorg. Chem.* **2007**, *46*, 10093−10107.

(27) Manriquez, J. M.; Yee, G. T.; McLean, R. S.; Epstein, A. J.; Miller, J. S. A room-temperature molecular/organic-based magnet. *Science* **1991**, *252*, 1415−1417.

(28) Saber, M. R.; Dunbar, K. R. Trigonal bipyramidal 5d-4f molecules with SMM behavior. *Chem. Commun.* **2014**, *50*, 2177−2179.

(29) Schelter, E. J.; Karadas, F.; Avendano, C.; Prosvirin, A. V.; Wernsdorfer, W.; Dunbar, K. R. A Family of Mixed-Metal Cyanide Cubes with Alternating Octahedral and Tetrahedral Corners Exhibiting a Variety of Magnetic Behaviors Including Single Molecule Magnetism. *J. Am. Chem. Soc.* **2007**, *129*, 8139−8149.
(30) Brown, A.; Saber, M.; Van den Heuvel, W.; Schulte, K.; Soncini, A.; Dunbar, K. R. Titanium(III) Member of the Family of Trigonal Building Blocks with Scorpionate and Cyanide Ligands. *Inorg. Chem.* **2017**, *56*, 1031−1035.
(31) Leung, W. H.; Che, C. M. Oxidation chemistry of ruthenium-salen complexes. *Inorg. Chem.* **1989**, *28*, 4619−4622.
(32) Guo, J. F.; Yeung, W. F.; Lau, P. H.; Wang, X. T.; Gao, S.; Wong, W. T.; Chui, S. S.; Che, C. M.; Wong, W. Y.; Lau, T. C. trans-$[Os^{III}(salen)(CN)_2]^-$: A New Paramagnetic Building Block for the Construction of Molecule-Based Magnetic Materials. *Inorg. Chem.* **2010**, *49*, 1607−1614.
(33) Zhang, D.; Zhao, Z.; Chen, K.; Chen, X. $[Co(salen)(CN)_2]^-$ as Building Block for the Design of Heterobimetallic Systems: Synthesis, Characterization, and Crystal Structures of Cyano-Bridged Co^{III}-Mn^{II} Complexes. *Synth. React. Inorg., Met.-Org., Nano-Met. Chem.* **2013**, *43*, 273−278.
(34) Albores, P.; Seeman, J.; Rentschler, E. Ferromagnetic coupled μ-phenoxo-μ-carboxylato heterodinuclear complexes based on the Cr(salen) moiety: structural and magnetic characterization. *Dalton Trans.* **2009**, 7660−7668.
(35) Man, W.-L.; Kwong, H.-K.; Lam, W. W. Y.; Xiang, J.; Wong, T.-W.; Lam, W.-H.; Wong, W.-T.; Peng, S.-M.; Lau, T.-C. General Synthesis of (Salen)ruthenium(III) Complexes via N···N Coupling of (Salen)ruthenium(VI) Nitrides. *Inorg. Chem.* **2008**, *47*, 5936−5944.
(36) Zhang, Q.; Zhou, H.; Shen, X.; Zhou, H.; Yang, Y. Syntheses, crystal structures and magnetic properties of four cyano-bridged bimetallic alternating chain complexes based on $[Cr^{III}(salen)(CN)_2]^-$ and $[Cr^{III}(bipy)(CN)_4]^-$ building blocks. *New J. Chem.* **2013**, *37*, 941−948.
(37) Zhang, D.; Wang, H.; Chen, Y.; Zhang, L.; Tian, L.; Ni, Z.-H.; Jiang, J. Synthesis, structure, and magnetic properties of cyanide-bridged low-dimensional heterometallic Fe^{III}-Mn^{II} complexes. *Dalton Trans.* **2009**, 9418−9425.
(38) Yeung, W. F.; Lau, P. H.; Lau, T. C.; Wei, H. Y.; Sun, H. L.; Gao, S.; Chen, Z. D.; Wong, W. T. Heterometallic $M^{II}Ru^{III}_2$ Compounds Constructed from trans-$[Ru(Salen)(CN)_2]^-$ and trans-$[Ru(acac)_2(CN)_2]^-$. Synthesis, Structures, Magnetic Properties, and Density Functional Theoretical Study. *Inorg. Chem.* **2005**, *44*, 6579−6590.
(39) Guo, J. F.; Wang, X. T.; Wang, B. W.; Xu, G. C.; Gao, S.; Szeto, L.; Wong, W. T.; Wong, W. Y.; Lau, T. C. One-Dimensional Ferromagnetically Coupled Bimetallic Chains Constructed with *trans*-$[Ru(acac)_2(CN)_2]^-$: Syntheses, Structures, Magnetic Properties, and Density Functional Theoretical Study. *Chem. - Eur. J.* **2010**, *16*, 3524−3535.
(40) Kashiwabara, K.; Katoh, K.; Ohishi, T.; Fujita, J.; Shibata, M. Preparation, and Structural and Spectroscopic Characterization of Cobalt(III) Phosphine Complexes of the Type, $[Co(CN)_{4-2n}(acac)_n(P)_2]^{(n-1)+}$ (acac = Acetylacetonate Ion, n = 0, 1, 2, and P = $P(CH_3)_x(C_6H_5)_{3-x}$, x = 0, 1, 2, 3). *Bull. Chem. Soc. Jpn.* **1982**, *55*, 149−155.
(41) Ohishi, T.; Kashiwabara, K.; Fujita, J. Preparation and Characterization of Cobalt(III)-Phosphine Complexes of the Type $[Co(CN)_2(acetylacetonate)(L)]$ (L - Tertiary 2-Aminoethylphosphines, and 1,2- and 1,3-Diphosphines). *Bull. Chem. Soc. Jpn.* **1983**, *56*, 1553−1554.
(42) Suzuki, T.; Kashiwabara, K.; Kita, M.; Fujita, J.; Kaizaki, S. Syntheses and crystal structures of geometrical isomeric pairs: trans- and cis-(PPh_4) $Co(acac)_2(CN)_2$ and trans- and cis-$Co(acac)_2(PMe_3$ or $PEt_3)_2$ PF_6 (acac = pentane-2,4-dionate). *Inorg. Chim. Acta* **1998**, *281*, 77−84.
(43) Toma, L. M.; Toma, L. D.; Delgado, F. S.; Ruiz-Perez, C.; Sletten, J.; Cano, J.; Clemente-Juan, J. M.; Lloret, F.; Julve, M. Trans-dicyanobis(acetylacetonato)ruthenate(III) as a precursor to build novel cyanide-bridged Ru^{III}-M^{II} bimetallic compounds [M = Co and Ni]. *Coord. Chem. Rev.* **2006**, *250*, 2176−2193.
(44) Yeung, W. F.; Lau, T. C.; Wang, X. Y.; Gao, S.; Szeto, L.; Wong, W. T. 2D $Ln^{III}Ru_2^{III}$ Compounds Constructed from trans-$[Ru(acac)_2(CN)_2]^-$. Syntheses, structures, and magnetic properties. *Inorg. Chem.* **2006**, *45*, 6756−6760.
(45) Chapman, K. W.; Southon, P. D.; Weeks, C. L.; Kepert, C. J. Reversible hydrogen gas uptake in nanoporous Prussian Blue analogues. *Chem. Commun.* **2005**, 3322−3324.
(46) Evans, D. F.; Missen, P. H. Water-soluble Schiff-base complexes of vanadyl(IV) and vanadium(III). *J. Chem. Soc., Dalton Trans.* **1987**, 1279−1281.
(47) Seidel, W.; Kreisel, G. Synthesis of 1,3-Diketonato Vanadium-(III) Halides. *Z. Anorg. Allg. Chem.* **1989**, *577*, 229−233.
(48) Manzer, L. E. New reagents for synthesis of paramagnetic organometallic, amide, and coordination-complexes of trivalent titanium, vanadium, and chromium. *Inorg. Chem.* **1978**, *17*, 1552−1558.
(49) Bonitatebus, P. J.K., Jr; Mandal, S. Synthesis and crystal structures of low-valent binuclear vanadium complexes using the tethering ligand m-xylylenebis(acetylacetonate) (m-xba^{2-}). *Chem. Commun.* **1998**, 939−940.
(50) Gambarotta, S.; Mazzanti, M.; Floriani, C.; Chiesi-Villa, A.; Guastini, C. Vanadium(III)-Schiff base complexes: a synthetic and structural study. *Inorg. Chem.* **1986**, *25*, 2308−2314.
(51) Hills, A.; Hughes, D. L.; Leigh, G. J.; Sanders, J. R. Reactions of vanadium(IV) halide complexes containing Schiff-base ligands with hydrazines; preparation and structure of [*N*,*N*′-ethylenebis-(salicylideneiminato)]bis-(phenylhydrazine)vanadium(III) iodide. *J. Chem. Soc., Dalton Trans.* **1991**, 325−329.
(52) Chilton, N. F.; Anderson, R. P.; Turner, L. D.; Soncini, A.; Murray, K. S. PHI: A powerful new program for the analysis of anisotropic monomeric and exchange-coupled polynuclear d- and f-block complexes. *J. Comput. Chem.* **2013**, *34*, 1164−1175.
(53) Shores, M. P.; Sokol, J. J.; Long, J. R. Nickel(II)-Molybdenum-(III)-Cyanide Clusters: Synthesis and Magnetic Behavior of Species Incorporating $[(Me_3tacn)Mo(CN)_3]$. *J. Am. Chem. Soc.* **2002**, *124*, 2279−2292.
(54) Liu, J.-L.; Pedersen, K. S.; Greer, S. M.; Oyarzabal, I.; Mondal, A.; Hill, S.; Wilhelm, F.; Rogalev, A.; Tressaud, A.; Durand, E.; Long, J. R.; Clerac, R. Access to Heteroleptic Fluorido-Cyanido Complexes with a Large Magnetic Anisotropy via Fluoride Abstraction. *Angew. Chem., Int. Ed.* **2020**, *59*, 10306−10310.
(55) Baker, M.; Blundell, S. J.; Domingo, N.; Hill, S. Spectroscopy Methods for Molecular Nanomagnets. *Struct. Bonding (Berlin, Ger.)* **2014**, *164*, 231−291.
(56) Hill, S. Magnetization tunneling in high-symmetry Mn_{12} single-molecule magnets. *Polyhedron* **2013**, *64*, 128−135.
(57) Hassan, A. K.; Pardi, L. A.; Krzystek, J.; Sienkiewicz, A.; Goy, P.; Rohrer, M.; Brunel, L. C. Ultrawide Band Multifrequency High-Field EMR Technique: A Methodology for Increasing Spectroscopic Information. *J. Magn. Reson.* **2000**, *142*, 300−312.
(58) Mola, M.; Hill, S.; Goy, P.; Gross, M. Instrumentation for millimeter-wave magnetoelectrodynamic investigations of low-dimensional conductors and superconductors. *Rev. Sci. Instrum.* **2000**, *71*, 186−200.
(59) Takahashi, S.; Hill, S. Rotating cavity for high-field angle-dependent microwave spectroscopy of low-dimensional conductors and magnets. *Rev. Sci. Instrum.* **2005**, *76*, 023114.
(60) Kittilstved, K. R.; Sorgho, L. A.; Amstutz, N.; Tregenna-Piggott, P. L. W.; Hauser, A. Ground-State Electronic Structure of Vanadium-(III) Trisoxalate in Hydrated Compounds. *Inorg. Chem.* **2009**, *48*, 7750−7764.
(61) Van Stappen, C.; Maganas, D.; DeBeer, S.; Bill, E.; Neese, F. Investigations of the Magnetic and Spectroscopic Properties of V(III) and V(IV) Complexes. *Inorg. Chem.* **2018**, *57*, 6421−6438.
(62) Beaulac, R.; Tregenna-Piggott, P. L. W.; Barra, A. L.; Weihe, H.; Luneau, D.; Reber, C. The electronic ground state of $[V(urea)_6]^{3+}$

https://dx.doi.org/10.1021/acs.inorgchem.0c01595
Inorg. Chem. 2020, 59, 13262−13269

probed by NIR luminescence, electronic Raman, and high-field EPR spectroscopies. *Inorg. Chem.* **2006**, *45*, 3399−3407.
(63) Tregenna-Piggott, P. L.; Weihe, H.; Bendix, J.; Barra, A. L.; Güdel, H. U. High-Field, Multifrequency EPR Study of the Vanadium(III) Hexaaqua Cation. *Inorg. Chem.* **1999**, *38*, 5928−5929.
(64) Bendix, J.; Brorson, M.; Schaffer, C. E. Accurate Empirical Spin-Orbit Coupling Parameters ζ_{nd} for Gaseous nd^q Transition Metal Ions. The Parametrical Multiplet Term Model. *Inorg. Chem.* **1993**, *32*, 2838−2849.
(65) Schäffer, C. E.; Jørgensen, C. K. The angular overlap model, an attempt to revive the ligand field approaches. *Mol. Phys.* **1965**, *9*, 401−412.

https://dx.doi.org/10.1021/acs.inorgchem.0c01595
Inorg. Chem. 2020, 59, 13262−13269